ISPRS Journal of Photogrammetry and Remote Sensing xxx (2015) xxx–xxx

Contents lists available at ScienceDirect

ISPRS Journal of Photogrammetry and Remote Sensing

journal homepage: www.elsevier.com/locate/isprsjprs

# Experimental Sentinel-2 LAI estimation using parametric, non-parametric and physical retrieval methods – A comparison

Jochem Verrelst [a,*], Juan Pablo Rivera [a], Frank Veroustraete [b], Jordi Muñoz-Marí [a], Jan G.P.W. Clevers [c], Gustau Camps-Valls [a], José Moreno [a]

[a] Image Processing Laboratory (IPL), Universitat de València, València, Spain
[b] Department of Bioscience Engineering, Faculty of Sciences, University of Antwerp, Antwerp, Belgium
[c] Laboratory of Geo-information Science and Remote Sensing, Wageningen University, Wageningen, The Netherlands

ARTICLE INFO

*Article history:*
Received 29 January 2015
Received in revised form 23 April 2015
Accepted 27 April 2015
Available online xxxx

*Keywords:*
Biophysical variables
Sentinel-2
Parametric
Non-parametric
Machine learning
Physically-based RTM inversion

ABSTRACT

Given the forthcoming availability of Sentinel-2 (S2) images, this paper provides a systematic comparison of retrieval accuracy and processing speed of a multitude of parametric, non-parametric and physically-based retrieval methods using simulated S2 data. An experimental field dataset (SPARC), collected at the agricultural site of Barrax (Spain), was used to evaluate different retrieval methods on their ability to estimate leaf area index (LAI). With regard to parametric methods, all possible band combinations for several two-band and three-band index formulations and a linear regression fitting function have been evaluated. From a set of over ten thousand indices evaluated, the best performing one was an optimized three-band combination according to $(\rho_{560} - \rho_{1610} - \rho_{2190})/(\rho_{560} + \rho_{1610} + \rho_{2190})$ with a 10-fold cross-validation $R^2_{CV}$ of 0.82 ($RMSE_{CV}$: 0.62). This family of methods excel for their fast processing speed, e.g., 0.05 s to calibrate and validate the regression function, and 3.8 s to map a simulated S2 image. With regard to non-parametric methods, 11 machine learning regression algorithms (MLRAs) have been evaluated. This methodological family has the advantage of making use of the full optical spectrum as well as flexible, nonlinear fitting. Particularly kernel-based MLRAs lead to excellent results, with variational heteroscedastic (VH) Gaussian Processes regression (GPR) as the best performing method, with a $R^2_{CV}$ of 0.90 ($RMSE_{CV}$: 0.44). Additionally, the model is trained and validated relatively fast (1.70 s) and the processed image (taking 73.88 s) includes associated uncertainty estimates. More challenging is the inversion of a PROSAIL based radiative transfer model (RTM). After the generation of a look-up table (LUT), a multitude of cost functions and regularization options were evaluated. The best performing cost function is Pearson's $\chi$-square. It led to a $R^2$ of 0.74 ($RMSE$: 0.80) against the validation dataset. While its validation went fast (0.33 s), due to a per-pixel LUT solving using a cost function, image processing took considerably more time (01:01:47). Summarizing, when it comes to accurate and sufficiently fast processing of imagery to generate vegetation attributes, this paper concludes that the family of kernel-based MLRAs (e.g. GPR) is the most promising processing approach.


## 1. Introduction

Spatio-temporally explicit, quantitative retrieval methods for vegetation bio-geophysical characteristics are a requirement in a variety of ecological and agricultural applications. Optical Earth observing satellites, endowed with a high temporal resolution, enable the retrieval and hence monitoring of plant bio-geophysical variables (Moulin et al., 1998; Dorigo et al., 2007). With forthcoming super-spectral Copernicus Sentinel-2 (S2) (Drusch et al., 2012) and Sentinel-3 missions (Donlon et al., 2012) an unprecedented data stream for land monitoring will soon become available to a diverse user community (Malenovsky et al., 2012; Berger et al., 2012). The expected vast Sentinel data stream will require enhanced processing techniques that are accurate, robust and fast.

In preparation to S2's launch, a wide variety of biophysical variable retrieval approaches dedicated to process the expected data stream have been proposed. These methods address retrieval of leaf chlorophyll content, leaf area index (LAI), canopy chlorophyll

* Corresponding author.
*E-mail address:* jochem.verrelst@uv.es (J. Verrelst).

http://dx.doi.org/10.1016/j.isprsjprs.2015.04.013
0924-2716/

content and fractional vegetation cover. Proposed methodologies using simulated S2 data range from vegetation indices (Delegido et al., 2011, 2013; Clevers and Kooistra, 2012; Hill, 2013; Schlemmera et al., 2013; Vincini et al., 2014) to machine learning regression algorithms (Verrelst et al., 2012b, 2013b; Rivera Caicedo et al., 2014a) until the inversion of radiative transfer methods (Richter et al., 2009; Atzberger and Richter, 2012; Rivera et al., 2013; Laurent et al., 2014; Verrelst et al., 2014). However, a pitfall with these studies is that they are based on different field datasets and study sites. Hence, the performance of the proposed retrieval methods cannot be quantitatively compared, and the validity of the different retrieval methods relative to the others remains unknown. Clearly, a systematic evaluation is a strong requirement.

Beyond S2 studies, biophysical variable retrieval methods can be categorized, typically in either of the following four general categories (Verrelst et al., submitted for publication):

1. *Parametric regression methods*: Parametric methods assume an explicit relationship between spectral observations and a bio-geophysical variable. Thus, explicit parameterized expressions are defined typically by utilizing statistical or physical knowledge of the variable to be extracted and the spectral response it induces. Typically a band arithmetic formulation is defined as a vegetation index and subsequently linked to the variable of interest based on a fitting function.
2. *Non-parametric regression methods*: Regression functions are directly determined by non-parametric methods, according to information derived from the available data without any assumption about data distribution or variable interrelations. In contrast with parametric regression methods, no explicit choice has to be made about spectral band relationships, transformation(s) or fitting functions.
3. *Physically-based methods*: Physically-based algorithms are applications of physical laws and applied to established cause-effect relationships. They infer model variables based on specific knowledge, such as that contained in radiative transfer functions.
4. *Hybrid methods*: Hybrid methods combine elements of statistical (typically non- parametric) and physically-based methods. Hybrid models exploit the generic properties of physically-based methods combined with the flexibility and computational efficiency of non-parametric non-linear regression methods.

Cited retrieval method categories have extensively been reviewed as well as qualitatively evaluated, based on the following general criteria: (1) potential to retrieve vegetation bio-geophysical properties; (2) the ability to generate multiple outputs; (3) the possibility to describe model transparency; (4) mapping speed; and, (5) the ability to provide retrieval uncertainties (Verrelst et al., this issue). No evaluation, however, of their performance was made because each of these methods was applied in different studies and hence used different datasets.

This brings us to the following main objective of this work: To quantitatively evaluate the predictive accuracy and processing speed of parametric, non-parametric and physically-based retrieval methods using identical datasets in the retrieval of a biophysical variable. By doing so, we evaluated the three method categories on their capability for LAI estimation. In principle, these methods are not restricted to a specific variable. In view of the expected S2 data stream, this study was applied to map LAI from experimental S2 data.

In the following sections we introduce first the generic parametric regression methods based on vegetation indices (Section 2.1). Subsequently, we introduce a broad range of nonparametric regression methods in Section 2.2, and finally we introduce radiative transfer model (RTM) inversion strategies in Section 2.3. Section 3 presents the experimental setup envisaged for comparing the different methods. Subsequently, Section 4 describes the application of the various methods in this study and their evaluation, while Section 5 presents accuracies, processing speed and mapping results. This paper closes with a discussion on the performance of the methods (Section 6) and conclusions (Section 7).

## 2. Methods

### 2.1. Parametric regression methods

Parametric regression methods explicitly determine parameterized expressions relating a limited number of spectral bands with vegetation bio-geophysical variables of interest. This family of approaches has long been most popular in optical Earth Observation, especially parameterized relations based on vegetation indices (VIs). VIs are defined with the objective to enhance spectral features sensitive to a vegetation property while reducing disturbance by combining a few spectral bands into a VI (Glenn et al., 2008). The principle basically entails mathematically defined combinations of spectral bands regressed with a bio-geophysical variable using a fitted function. The problem with this approach is that decisions have to be made that may impact on the performance of the estimation: i.e. band selection, index formulation and type of fitting function (Rivera Caicedo et al., 2014b).

Prior to the selection of a VI model for the retrieval of biophysical variables from remote sensing imagery, a systematic assessment of possible band combinations, VI formulations and curve fitting procedures is required. An attractive approach therefore is calculating all possible band combinations according to VI formulations. For instance, the most often applied vegetation index is the generic Normalized Difference Index ($NDI_{a,b}$). The NDI calculates all possible two-band narrowband combinations according to the formulation:

$$NDI_{a,b} = (\rho_b - \rho_a)/(\rho_b + \rho_a) \quad (1)$$

where $\rho_{a,b}$ is reflectance in the a and b bands for the entire optical spectral range. These so-called generic spectral indices permit the selection of a best performing index when correlated with a biogeophysical variable using a validation dataset. With regard to vegetation or spectral index formulation (VI or SI), an extensive review was conducted by le Maire et al. (2004). Typically, indices can be classified into four categories:

1. Indices using a single reflectance or a difference between reflectances at two wavelengths;
2. Simple ratio of reflectances (SR);
3. Normalized difference ratios of reflectances (ND);
4. Indices based on reflectance signature derivatives.

These indices can be generalized by evaluating them for all optical wavelengths. Most of them rely on two-band formulations. A typical problem of two-band spectral indices is that they rapidly lead to saturated values of the biophysical property in question. This can be partly overcome, by optimizing band selection (Delegido et al., 2011, 2013). Alternatively, three-band spectral indices (3BSIs) have been proposed to avoid the saturation problem in many two-band spectral indices (Wang et al., 2012). Table 1 provides common types of published indices as identified by le Maire et al. (2004) and more authors who published more recently.

Please cite this article in press as: Verrelst, J., et al. Experimental Sentinel-2 LAI estimation using parametric, non-parametric and physical retrieval methods – A comparison. ISPRS J. Photogram. Remote Sensing (2015), http://dx.doi.org/10.1016/j.isprsjprs.2015.04.013

**Table 1**
Common types of published indices as identified by le Maire et al. (2004) and other authors (see 'Source'). In the table *a*, *b*, and *c* represent wavelengths.

| Based on | Type | Formula | Source |
|---|---|---|---|
| Reflectances | $\rho$ | $\rho_a$ | |
| Reflectances | SR | $\rho_a/\rho_b$ | |
| Reflectances | ND | $(\rho_a-\rho_b)/(\rho_a+\rho_b)$ | |
| Reflectances | mSR | $(\rho_a-\rho_c)/(\rho_b-\rho_c)$ | |
| Reflectances | mND | $(\rho_a-\rho_b)/(\rho_a+\rho_b-2\rho_c)$ | |
| Reflectances | 3BSI | $(\rho_a-\rho_c)/(\rho_b+\rho_c)$ | This study |
| Reflectances | 3BSI Wang | $(\rho_a-\rho_b+2\rho_c)/(\rho_a+\rho_b-2\rho_c)$ | Wang et al. (2012) |
| Reflectances | 3BSI Tian | $(\rho_a-\rho_b-\rho_c)/(\rho_a+\rho_b+\rho_c)$ | Tian et al. (2013) |
| Derivatives | DVI | $\rho_a-\rho_b$ | |

**Table 2**
Evaluated non-parametric regression algorithms.

| Name algorithm | Core algorithm | Source |
|---|---|---|
| Principal component regression (PCR) | Matrix inversion | Wold et al. (1987) |
| Partial least squares regression (PLSR) | Matrix inversion | Geladi and Kowalski (1986) |
| Neural Network (NN) | Levenberg–Marquardt algorithm | Hagan and Menhaj (1994) |
| Regression tree (RT) | Sorting & grouping | Breiman et al. (1984) |
| Boosting trees (BoT) | Least squares boosting + RT | Friedman et al. (2000) |
| Bagging trees (BaT) | Bootstrap aggregation (bagging) + RT | Breiman (1996) |
| Relevance vector machine (RVM) | Bayesian statistical inference | Tipping (2001) |
| Extreme learning machine (ELM) | Pseudo matrix inversion | Huang et al. (2006) |
| Kernel ridge regression (KRR) | Matrix inversion | Suykens and Vandewalle (1999) |
| Gaussian processes regression (GPR) | Bayesian statistical inference | Rasmussen and Williams (2006) |
| Variational Heteroscedastic (VH) GPR (VH-GPR) | Bayesian statistical inference | Lazaro-Gredilla et al. (2013) |

These indices are subsequently correlated to field data of a variable of interest, e.g. LAI. Regarding selected fitting functions, a variety of functions (e.g., linear, exponential, logarithmic, polynomial) have been evaluated in Rivera Caicedo et al. (2014b). The impact of fitting functions as opposed to the impact of band selection appeared to be marginal. Therefore, in this paper we restricted the fitting method to ordinary least-squares linear regression.

### 2.2. Non-parametric regression methods

Non-parametric algorithms are optimized with a training phase based on existing data. These include model weights (coefficients), which are adjusted to minimize the estimation error of the variables to be extracted. An important advantage of this methodology is that it is usually based on full optical spectral datasets, i.e. they make use of all available optical spectral information.

To develop regression models with an optimal generic capacity requires that their data structure has to be exploited efficiently. This typically requires the definition of a flexible model able to combine the different data structure features in a non-linear way. Non-parametric algorithms can be split into linear and non-linear regression methods, the latter is also commonly referred to as machine learning regression algorithms (MLRAs) (see Verrelst et al. (2012b)).

A list of evaluated non-parametric regression methods is provided in Table 2. More information about their algorithms can be found in the cited papers. A comprehensive description is provided in Verrelst et al. (this issue). The algorithms have been brought together in one toolbox, called SimpleR (Camps-Valls et al., 2013) available at http://www.uv.es/gcamps/code/simpleR.html.

### 2.3. Physically based methods

Physically-based model inversion methodologies are based on physical laws and established, well-founded, physical knowledge of variable relationships. The inversion of a physically-based canopy RTM with actual (full-spectrum) remote sensing data is considered as a physically sound approach for the retrieval of bio-geophysical variables of terrestrial surfaces because the approach is generic (Dorigo et al., 2007). Nevertheless, these approaches are not straightforward. The inversion of canopy RTMs is intrinsically undetermined and hence ill-posed. This makes physically-based retrievals of vegetation properties a challenging task. Several strategies have been proposed to mitigate the problem of ill-posedness, most of them relying on lookup-table (LUT)-based inversion strategies (e.g. Knyazikhin et al., 1998; Weiss et al., 2000; Darvishzadeh et al., 2008). LUT-based inversion requires simulations of the spectral reflectances for a large yet limited range of RTM variable values. The inversion problem is thereby transformed into the identification of a modeled reflectance set most resembling a measured one, querying the LUT (Liang, 2007). A LUT query is typically performed by applying a cost function. The cost function generates a value for one or multiple RTM input variables set by minimizing the summed differences between simulated and measured reflectances for all wavelengths. Various regularization strategies have been proposed to optimize the robustness of the LUT-based inversion routines (Verrelst et al., submitted for publication). For instance:

1. The use of the mean or median of multiple best solutions in the inversion, as opposed to a single best solution (Combal et al., 2002; Richter et al., 2009; Darvishzadeh et al., 2011; Verrelst et al., 2014); and
2. The addition of Gaussian noise to account for uncertainties linked to measurements and models (Richter et al., 2009, 2011; Verrelst et al., 2014).

Another widely applied regularization technique is the introduction of a priori information, e.g. per land cover type. This technique is not tested here since we focus only on methods immediately applicable to the complete image. Alternatively, different cost functions deal with different distribution classes, allowing us to deal with outliers and non-linear distortions in a better way than the commonly used least squares estimation distance (LSE) (Rivera et al., 2013; Verrelst et al., 2014). A wide range of distances/metrics has been developed in the fields of mathematics, statistics and physics. They all represent the "closeness" between two functions, though the nature of these functions can be different (Leonenko et al., 2013). Most of these functions require one

Please cite this article in press as: Verrelst, J., et al. Experimental Sentinel-2 LAI estimation using parametric, non-parametric and physical retrieval methods – A comparison. ISPRS J. Photogram. Remote Sensing (2015), http://dx.doi.org/10.1016/j.isprsjprs.2015.04.013

or two parameters to be tuned. That may hamper their use in operational processing chains. Therefore only those cost functions without additional parameters were analyzed in earlier work (Rivera et al., 2013). It led to a selection of 10 potentially promising cost functions. To describe the problem in a statistical way let us accept that $D[P,Q]$ represents the distance between two functions, where $P=(p(\lambda_1),\ldots,p(\lambda_n))$ is the reflectance signature derived from satellite data and $Q=(q(\lambda_1),\ldots,q(\lambda_n))$ is the LUT containing simulated reflectances with $\lambda_1,\ldots,\lambda_n$ representing $n$ spectral bands. The purpose is to find the best estimate by solving the minimization problem using different statistical distances as presented in Table 3.

## 3. Experimental and simulated data

### 3.1. Sentinel-2

ESA's S2 satellites capitalize on technology and experience acquired with the SPOT and Landsat missions dating from the past decades (Drusch et al., 2012). S2 is a polar-orbiting, super-spectral high-resolution imaging mission. The mission is envisaged to fly a pair of satellites, with the first planned to be launched in 2015. Each S2 satellite carries a Multi-Spectral Imager (MSI) with a swath width of 290 km. It provides a versatile set of 13 spectral bands spanning from the visible and near infrared (VNIR) to the short-wave infrared (SWIR), featuring four bands at 10 m, six bands at 20 m and three bands at 60 m spatial resolution (Table 4). S2 incorporates three bands in the red-edge region, centered at 705, 740 and 783 nm. The S2 satellite pair aims at delivering data from all land surfaces and coastal zones every five days and under cloud-free conditions, and typically every 15–30 days considering the presence of clouds. To serve the objectives of Copernicus (The European Earth Observation Programme) S2 satellites will provide data for the generation of high-level operational products (level 2b/3) such as land-cover and land-change detection maps and geophysical variables maps.

### 3.2. Field data

To quantitatively compare the three different categories of retrieval methods cited earlier, a joint reference dataset is to be used. For this purpose the widely used SPARC dataset (Delegido et al., 2011, 2013) is chosen. The SPectra bARrax Campaign (SPARC) field dataset encompasses different crop types, growing phases, canopy geometries and soil conditions. The SPARC-2003 campaign took place from 12 to 14 July in Barrax, La Mancha, Spain (coordinates 30°3′N, 28°6′W, 700 m altitude). Bio-geophysical parameters have been measured within a total of 108 Elementary Sampling Units (ESUs) for different crop types (garlic, alfalfa, onion, sunflower, corn, potato, sugar beet, vineyard and wheat). An ESU refers to a plot, which is sized compatible with pixel dimensions of about 20 m × 20 m. In the analysis no differentiation between crops was made.

Green LAI has been derived from canopy measurements made with a LiCor LAI-2000 digital analyzer. Each ESU was assigned one LAI value, obtained as a statistical mean of 24 measurements (8 data readings × 3 replica) with standard errors ranging from 5% to 10% (Fernández et al., 2005). Strictly speaking, assuming a random leaf angle distribution, the impact of clumping has been assessed only partially using the LiCor and its corresponding software. Hence, effective LAI is given as an output variable. For all ESUs, LAI ranges from 0.4 to 6.2 ($m^2$ single sided leaf surface)/($m^2$ ground surface). To be able to compare statistical methods with the physical method, bare soils were not included in the validation dataset since the inversion of canopy RTMs is only relevant for fully vegetated land cover types.

During the campaign, airborne hyperspectral HyMap flight-lines were acquired for the study site, during the month of July 2003. HyMap flew with a configuration of 125 contiguous spectral bands, spectrally positioned between 430 and 2490 nm. Spectral bandwidth varied between 11 and 21 nm. The pixel size at overpass was 5 m. The flight-lines were corrected for radiometric and atmospheric effects according to the procedures of Alonso and Moreno (2005) and Guanter et al. (2005). A RGB map of the used flight-line is provided in Fig. 5.

Finally, a calibration dataset was prepared, referring to the centre point of each ESU and its corresponding LAI values. HyMap data were then spectrally resampled to the band settings of S2. Note that the spatial size of HyMap is kept as such that no spatial information is lost when interpreting the maps obtained.

## 4. Methods application and evaluation

### 4.1. Cross-validation sampling for parametric and non-parametric regression

Field data are required for the parametric and non-parametric methods to be trained and calibrated, resulting in a fitting function between vegetation index values and LAI measurements. The validation of these methods was based on a $k$-fold cross-validation technique (Snee, 1977). The $k$-fold cross-validation requires the dataset to be randomly divided into $k$ equal-sized sub-datasets. From these $k$ sub-datasets, $k$-1 sub-datasets are selected as a training dataset and a single $k$ sub-dataset is used as a validation dataset for model testing. The cross-validation process is then repeated $k$ times, with each of the $k$ sub-datasets used as a validation dataset. The results from each of these iterative validation steps are then combined to produce a single estimation value. This way, all data are used for both training and validation, and each single observation is used for validation exactly once. In this study, we used a 10-fold ($k$ = 10) cross-validation procedure.

### 4.2. LUT-based inversion strategy

With regard to RTM inversion approaches, the full SPARC field dataset was used to evaluate the various LUT-based inversion strategies. Hence, contrary to the approaches discussed earlier, the full field dataset was used only for validation purposes, i.e. no need for a cross-validation sampling.

The simulated dataset has been produced by coupling the PROSPECT-4 with the 4SAIL RTM's. These coupled RTM's are fast, invertible and do represent homogeneous plant cover well on flat surfaces such as those present at Barrax. Both models, commonly referred to as PROSAIL, have been used extensively over the past few years for a variety of applications (Jacquemoud et al., 2009). PROSPECT-4 simulates leaf reflectance and transmittance for the optical spectrum from 400 to 2500 nm with a 1 nm spectral resolution and as a function of biochemistry and anatomical structure of the canopy and its leaves. It consists of four parameters, being leaf structure, leaf chlorophyll content (LCC), equivalent water thickness and dry matter content (Feret et al., 2008). 4SAIL calculates top-of-canopy reflectance. The 4SAIL input variables are: LAI, leaf angle distribution, the diffuse/direct irradiation ratio, a hotspot parameter and the sun-target-sensor geometry. The spectrally dependent input consists of leaf reflectance and transmittance, as simulated with PROSPECT-4 and a moist and dry soil reflectance spectrum. The soil spectra are an average of bare soil spectral signatures as calculated from bare moist and dry soil pixels identified in the imagery.

The imposed boundaries and distributions of the PROSAIL variables are illustrated in Table 5. These were obtained from the

Please cite this article in press as: Verrelst, J., et al. Experimental Sentinel-2 LAI estimation using parametric, non-parametric and physical retrieval methods – A comparison. ISPRS J. Photogram. Remote Sensing (2015), http://dx.doi.org/10.1016/j.isprsjprs.2015.04.013

**Table 3**
Ten cost functions used in the current study.

| Cost function | Algorithm |
|---|---|
| Least absolute error | $D(P,Q)=\sum_{\lambda_l=1}^{\lambda_n}\lvert p(\lambda_l)-q(\lambda_l)\rvert$ |
| Shannon (1948) | $D(P,Q)=-\sum_{\lambda_l=1}^{\lambda_n}\left(\frac{p(\lambda_l)+q(\lambda_l)}{2}\right)\log\left(\frac{p(\lambda_l)+q(\lambda_l)}{2}\right)+\frac{1}{2}\left(\sum_{\lambda_l=1}^{\lambda_n}p(\lambda_l)log(p(\lambda_l))+\sum_{\lambda_l=1}^{\lambda_n}q(\lambda_l)log(q(\lambda_l))\right)$ |
| L-divergence lin | $D[P,Q]=\sum_{\lambda_l=1}^{\lambda_n}p(\lambda_l)\ln(p(\lambda_l)+q(\lambda_l))\ln(q(\lambda_l)-(p(\lambda_l)+q(\lambda_l)))\ln\left(\frac{p(\lambda_l)+q(\lambda_l)}{2}\right)$ |
| Bhattacharyya divergence | $D[P,Q]=-\log\left(1+\sum_{\lambda_l=1}^{\lambda_1}\sqrt{p(\lambda_l)q(\lambda_l)}-\frac{1}{2}(p(\lambda_l)+q(\lambda_l)\right)$ |
| Jeffreys–Kullback–Leibler | $D[P,Q]=\sum_{\lambda_l=1}^{\lambda_n}(p(\lambda_l)-q(\lambda_l))(\ln(p(\lambda_l))-\ln(q(\lambda_l)))$ |
| Neyman chi-square | $D[P,Q]=\sum_{\lambda_l=1}^{\lambda_n}\frac{(p(\lambda_l)-q(\lambda_l))^2}{q(\lambda_l)}$ |
| Pearson chi-square | $D[P,Q]=\sum_{\lambda_l=1}^{\lambda_n}\frac{(q(\lambda_l)-p(\lambda_l))^2}{p(\lambda_l)}$ |
| Normal distrubution-LSE | $D[P,Q]=\sum_{\lambda_l=1}^{\lambda_n}(p(\lambda_l)-q(\lambda_l))^2$ |
| Geman and McClure | $D(P,Q)=\sum_{\lambda_l=1}^{\lambda_n}\frac{(p(\lambda_l)-q(\lambda_l))^2}{(1+(p(\lambda_l)-q(\lambda_l))^2)}$ |
| Exponential | $D[P,Q]=\sum_{\lambda_l=1}^{\lambda_n}q(\lambda_l)\left(\exp\left(-\frac{p(\lambda_l)-q(\lambda_l)}{q(\lambda_l)}\right)-1\right)$ |

**Table 4**
Sentinel-2 MSI band settings.

| Band # | B1 | B2 | B3 | B4 | B5 | B6 | B7 | B8 | B8a | B9 | B10 | B11 | B12 |
|---|---|---|---|---|---|---|---|---|---|---|---|---|---|
| Band center (nm) | 443 | 490 | 560 | 665 | 705 | 740 | 783 | 842 | 865 | 945 | 1375 | 1610 | 2190 |
| Band width (nm) | 20 | 65 | 35 | 30 | 15 | 15 | 20 | 115 | 20 | 20 | 30 | 90 | 180 |
| Spatial resolution (m) | 60 | 10 | 10 | 10 | 20 | 20 | 20 | 10 | 20 | 60 | 60 | 20 | 20 |

**Table 5**
Range and distribution of input parameters used to establish the synthetic canopy reflectance database for use in the LUT.

| Model parameters | | Units | Range | Distribution |
|---|---|---|---|---|
| *Leaf parameters: PROSPECT-4* | | | | |
| $N$ | Leaf structure index | Unitless | 1.3–2.5 | Uniform |
| LCC | Leaf chlorophyll content | [μg/cm$^2$] | 5–75 | Gaussian ($\bar{x}$: 35, SD: 30) |
| $C_m$ | Leaf dry matter content | [g/cm$^2$] | 0.001–0.03 | Uniform |
| $C_w$ | Leaf water content | [cm] | 0.002–0.05 | Uniform |
| *Canopy variables: 4SAIL* | | | | |
| LAI | Leaf area index | [m$^2$/m$^2$] | 0.1–7 | Gaussian ($\bar{x}$: 3, SD: 2) |
| $\alpha_{soil}$ | Soil scaling factor | Unitless | 0–1 | Uniform |
| ALA | Average leaf angle | [°] | 40–70 | Uniform |
| HotS | Hot spot parameter | [m/m] | 0.05–0.5 | Uniform |
| skyl | Diffuse incoming solar radiation | [fraction] | 0.05 | – |
| $\theta_s$ | Sun zenith angle | [°] | 22.3 | – |
| $\theta_v$ | View zenith angle | [°] | 20.19 | – |
| $\phi$ | Sun-sensor azimuth angle | [°] | 0 | – |

Similar variable ranges/values/distributions were used according to field configurations and related studies (Rivera et al., 2013; Verrelst et al., 2014). $\bar{x}$: mean, SD: standard deviation.

measurement campaigns and/or other studies which used the same crops (Rivera et al., 2013; Verrelst et al., 2014). The boundary conditions were selected to describe the characteristics of all crop types used in the study, with each variable 10 times sampled. Gaussian input distributions were generated for LAI and LCC to put more emphasis on the variable values being present in the actual growth stages of the crops. These variables were 100 times sampled. Sun and viewing conditions correspond with the measuring conditions at satellite overpass. All possible combinations have been calculated from the leaf and canopy input ranges as defined in Table 5. Since the sum of all the combinations led to an unrealistically large number of simulations (10 billion), a LUT size of 10,000 TOC (Top-Of-Canopy) reflectance realizations has been randomly chosen in accordance with the approach of Darvishzadeh et al. (2012).

Similarly as in Rivera et al. (2013) and Verrelst et al. (2014), apart from the evaluated cost functions (Table 3) also the addition of a Gaussian noise component and the occurrence of multiple solutions in the inversion were investigated. A range of 0–20% noise (with steps of 1%) applied to the simulations and a mean of multiple solutions of best matching simulated spectra with a range of 0–5% (with steps of 0.25%) were evaluated on inversion efficiency impact.

### 4.3. ARTMO and retrieval validation

This study was conducted within an in-house software package named ARTMO (Automated Radiative Transfer Models Operator) (Verrelst et al., 2012c). ARTMO embodies a suite of leaf and canopy radiative transfer models (RTMs) including PROSAIL and several retrieval toolboxes, i.e. a spectral indices toolbox, (Rivera Caicedo et al., 2014b), a machine learning regression algorithm toolbox (Rivera Caicedo et al., 2014a), and a LUT-based inversion toolbox (Rivera et al., 2013). The ARTMO package runs in MATLAB and can be downloaded at: http://ipl.uv.es/artmo/.

The ability of parametric and non-parametric estimation was evaluated by examining the cross-validation estimate of the root-mean-squared error (RMSE) and the coefficient of determination ($R^2$), which are averaged 10-fold. For the RTM inversion

**Table 6**
Cross-validation statistics (mean ($\bar{x}$) and standard deviation (SD) of $RMSE_{CV}$ and $R^2_{CV}$) and processing speed for the best performing index per index formulation. Results are ranked according to $R^2_{CV}$.

| Index name | Formulation | Best bands | $RMSE_{CV}$ $mu_x$ (SD) | $R^2_{CV}$ $\bar{x}$ (SD) | Processing speed (s) |
|---|---|---|---|---|---|
| 3BSI Tian | $(\rho_a - \rho_b - \rho_c)/(\rho_a + \rho_b + \rho_c)$ | $\rho_a$: 560, $\rho_b$: 1610, $\rho_c$: 2190 | 0.615 (0.123) | 0.823 (0.114) | 0.118 |
| mND | $(\rho_a - \rho_b)/(\rho_a + \rho_b - 2\rho_c)$ | $\rho_a$: 560, $\rho_b$: 1610, $\rho_c$: 2190 | 0.671 (0.114) | 0.792 (0.110) | 0.065 |
| mSR | $(\rho_a - \rho_c)/(\rho_b - \rho_c)$ | $\rho_a$: 560, $\rho_b$: 1375, $\rho_c$: 2190 | 0.686 (0.107) | 0.787 (0.114) | 0.063 |
| 3BSI | $(\rho_a - \rho_c)/(\rho_b + \rho_c)$ | $\rho_a$: 560, $\rho_b$: 1375, $\rho_c$: 2190 | 0.691 (0.107) | 0.776 (0.116) | 0.039 |
| SR | $\rho_a/\rho_b$ | $\rho_a$: 443, $\rho_b$: 560 | 0.725 (0.202) | 0.766 (0.142) | 0.020 |
| DVI | $\rho_a - \rho_b$ | $\rho_a$: 560, $\rho_b$: 2190 | 0.748 (0.112) | 0.740 (0.149) | 0.036 |
| 2BSI | $(\rho_b - \rho_a)/(\rho_b + \rho_a)$ | $\rho_a$: 1610, $\rho_b$: 2190 | 0.777 (0.130) | 0.739 (0.144) | 0.020 |
| 3BSI Wang | $(\rho_a - \rho_b + 2\rho_c)/(\rho_a + \rho_b - 2\rho_c)$ | $\rho_a$: 443, $\rho_b$: 560, $\rho_c$: 665 | 0.770 (0.125) | 0.730 (0.133) | 0.051 |
| $R$ | $\rho_a$ | $\rho_a$: 865 | 0.923 (0.123) | 0.618 (0.129) | 0.037 |

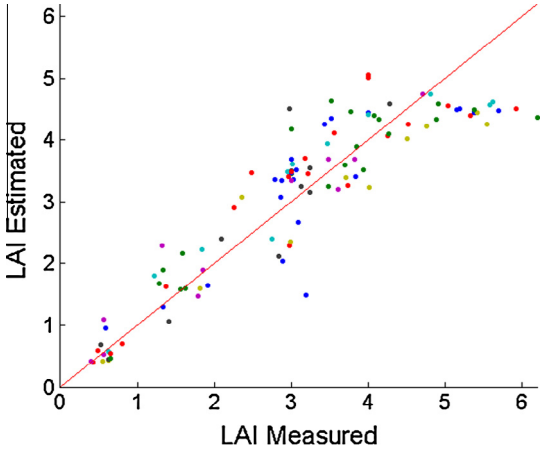


**Fig. 1.** Measured vs. estimated LAI values along the 1:1-line of the best performing VI model (see Table 6). The different colors indicate the 10-fold subsets. (For interpretation of the references to colour in this figure legend, the reader is referred to the web version of this article.)

strategies RMSE and $R^2$ were calculated directly using all validation data. Processing speed of the retrieval methods and mapping were logged as well. All analysis was performed using a 64 bit processor (Intel® Core™ i7-4700MQ CPU@ 2.40 GHz, 16 GB RAM).

## 5. Results

### 5.1. Parametric regression based on vegetation indices

All possible band combinations for the two-band and three-band formulations according to Table 1 have been analyzed for the S2 bands using the SPARC field dataset. Because of the large number of band combinations (156 for two-band combinations and 2041 for three-band combinations) only the best performing index per formulation is listed in Table 6. Multiple indices per formulation may perform almost equally well, but the overall goal of this study was to compare in particular the different categories of retrieval methods. Therefore, best performing combinations are presented only. In total, 10,686 indices have been evaluated. Generally, the best-performing three band indices outperformed the more conventional best-performing two-band indices. This implies that there is no reason to limit this exercise to two-band indices. Only the three-band index according to Wang et al. (2012) performed more poorly than the two-band indices. Another observation is that the type of formulation can play an important role. When inspecting the standard deviation (SD) of the cross-variation results, the simple ratio (SR) formulation performed considerably less stable (i.e. larger SD) than normalized formulations. Regarding three-band normalized formulations, the 3BSI according to Tian et al. (2013) proved to perform more successful than the other types of 3BSI formulations with about the same stability. The index was optimized as follows: $(\rho_{560} - \rho_{1610} - \rho_{2190})/(\rho_{560} + \rho_{1610} + \rho_{2190})$. From Table 6 it is shown that the selected spectral bands are encountered as well in other optimized indices. All indices - due to their simplicity - have in common that they are extremely fast in processing. The 10 $k$-fold cross-validation calibration and validation of the functions occurred practically instantly.

The scatter plot of estimated versus measured LAI values is shown in Fig. 1. Despite a relatively high $R^2_{CV}$ (0.82) it can be noted that LAI saturation at high LAI values still occurs. It again underlines the minor ability of indices in dealing with LAI estimates of densely packed canopies. However, other curve fitting types (e.g. exponential, polynomial, logarithmic) or indices with four or more bands may be able to alleviate this problem somewhat (Rivera Caicedo et al., 2014b).

### 5.2. Non-parametric regression algorithms

Table 7 displays the cross-validation results of the non-parametric regression algorithms for the S2 bands using the SPARC dataset, again ranked according to $R^2_{CV}$ results. Of interest is that the large majority of non-parametric regression algorithms outperforms the vegetation indices, especially the (nonlinear) machine learning algorithms (MLRAs). Most of these MLRAs are from the family of kernel methods. These are characterized by non-linear transformations. Top-performing MLRAs are variational heteroscedastic Gaussian processes regression (VH-GPR) and kernel ridge regression (KRR), bagging trees, relevance vector machine (RVM) and extreme vector machine (EVM). These methods explain about 90% of observed variance in LAI. Particularly the excellent performing algorithms KRR and the GPR families are of interest. KRR is of interest because of its high processing speed, especially because, unlike GPR, only a kernel parameter is used and thus the covariance (kernel) function is far more simple. GPR is of interest, even though it is computationally more demanding, due to its ability to provide additional information such as ranking of relevant bands as well as uncertainties (Verrelst et al., 2012b,a). Though still providing accurate estimates, neural networks (NN) and RVM are considerably slower. NN was rather slow when developing a model because many hyperparameters were to be tuned (number of hidden units, learning rate, and momentum term). The linear non-parametric regression models such as principal component regression (PCR) and partial least squares regression (PLSR), while being extremely fast, performed considerably poorer than their nonlinear counterparts. These methods cannot cope with complex nonlinear relations.

**Table 7**
Cross-validation statistics (mean ($\bar{x}$) and standard deviation (SD) of $RMSE_{CV}$ and $R^2_{CV}$) and processing speed for each non-parametric regression algorithm. Results are ranked according to $R^2_{CV}$.

| Algorithm | $RMSE_{CV}$ $\bar{x}$ (SD) | $R^2_{CV}$ $\bar{x}$ (SD) | Processing speed (s) |
|---|---|---|---|
| VH-Gaussian processes regression (VH-GPR) | 0.436 (0.137) | 0.902 (0.085) | 1.695 |
| Gaussian processes regression (GPR) | 0.440 (0.132) | 0.900 (0.085) | 0.767 |
| Kernel ridge regression (KRR) | 0.453 (0.127) | 0.897 (0.079) | 0.092 |
| Bagging trees (BaT) | 0.472 (0.119) | 0.887 (0.085) | 1.380 |
| Relevance vector machine (RVM) | 0.458 (0.129) | 0.886 (0.081) | 28.322 |
| Extreme learning machine (ELM) | 0.506 (0.124) | 0.879 (0.072) | 0.780 |
| Neural Network (NN) | 0.561 (0.160) | 0.849 (0.092) | 4.614 |
| Partial least squares regression (PLSR) | 0.584 (0.126) | 0.827 (0.123) | 0.010 |
| Boosting trees (BoT) | 0.619 (0.152) | 0.826 (0.084) | 0.947 |
| Regression tree (RT) | 0.601 (0.169) | 0.825 (0.147) | 0.089 |
| Principal component regression (PCR) | 0.803 (0.141) | 0.686 (0.144) | 0.003 |

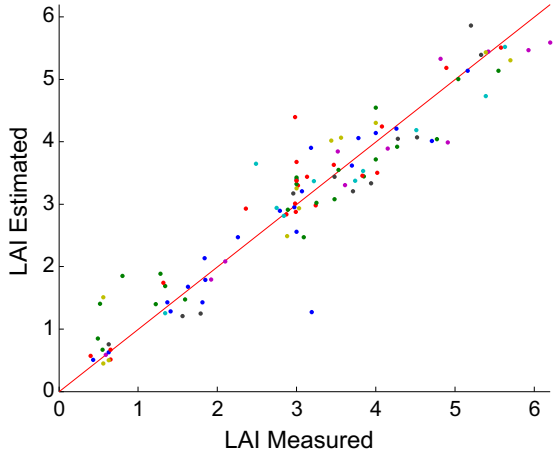


**Fig. 2.** Measured vs. estimated LAI values along the 1:1-line of the best performing non-parametric model (see Table 7). The different colors indicate the 10-fold subsets.

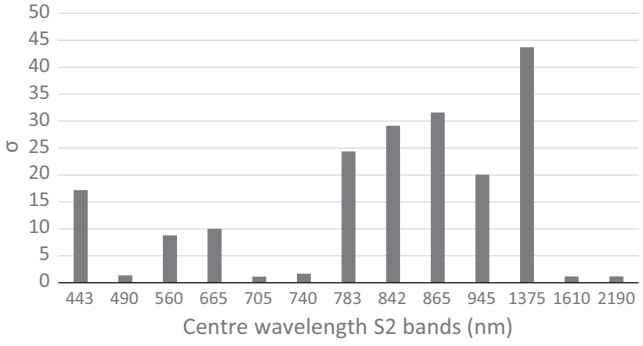


**Fig. 3.** Sigmas of the generated VH-GPR model. The lower the sigma the more important the band.

Compared to VI-results, it can be suggested that the majority of non-parametric regression methods perform more stable than the parametric methods when considering the lower standard deviations (SD) of the $R^2_{CV}$ results. That is also visualized in the scatter plot of the best performing method, VH-GPR (Fig. 2). This MLRA is well able to overcome the saturation effect. Apart from a few outliers, all estimates are closer to the 1:1-line, even for LAI measurements above 5. Especially the very low LAI value estimates (<1) are accurately predicted. The same excellent performance was observed for the GPR and KRR approaches. Another interesting feature of the GPR family to inspect is their ability to provide insight in band relevance when developing the regression model. Differences between samples are given by GPRs for each band typically using a covariance function defined as: $K(x_i, x_j) = exp\left(-\frac{\|\mathbf{x}_i - \mathbf{x}_j\|^2}{2\sigma^2}\right)$. The $\sigma$ can be interpreted as the relevance of band $b$. Intuitively, high values of $\sigma$ mean that relations largely extend along that band, hence suggesting a lower informative content. On the other hand, the lower the $\sigma$ the more relevant the band (Verrelst et al., 2012a,b). This is also illustrated in Fig. 3. Of interest is that the most relevant bands were encountered in the red edge and the SWIR, which is in agreement with earlier observations (Delegido et al., 2011, 2013; Rivera Caicedo et al., 2014b).

### 5.3. LUT-based RTM inversion

LUT-based RTM inversion is a challenging exercise because a RTM has to be selected first, then a LUT has to be configured together with a cost function and finally regularization options have to be defined. These decisions may impact the inversion performance. Here we report on the evaluation of 10 cost functions. The best-performing configurations per cost function are listed in Table 8 again sorted according to the $R^2$ statistic. Additionally, *RMSE* and processing speed are provided. At best, a $R^2$ of 0.74 is obtained, which is similar to that of the two-band indices. However, to achieve the best performance results, the insertion of quite some noise to the simulated data was required. It accounts for the uncertainties linked to measurements and LUT configuration. Typical for this case is that the $R^2$ is comparable with the performance of two-band indices but RMSE is significantly higher than the $RMSE_{CV}$ of vegetation indices (Table 6). Inversion processing is relatively fast (each inversion scheme <1 s), but still about ten times slower than when vegetation indices are used.

Two interesting observations can be made from Fig. 4. First, the inversion scheme faces difficulties, when sparsely vegetated surfaces are retrieved. Samples with LAI measurements below a value of one are systematically overestimated. This may be due to a poor selection of bare soil profiles in the LUT generation, inducing mismatching. A second observation deals with densely vegetated surfaces. LAI measurements above four are systematically underestimated by the inversion scheme. This is suggested to be due to saturation effects, a well-known phenomenon with PROSAIL simulations (Bacour et al., 2006; Weiss et al., 2007; Garrigues et al., 2008). Both over- and under-estimations demonstrate that LUT-based inversions are a challenging approach, requiring optimizations for many aspects.

Please cite this article in press as: Verrelst, J., et al. Experimental Sentinel-2 LAI estimation using parametric, non-parametric and physical retrieval methods – A comparison. ISPRS J. Photogram. Remote Sensing (2015), http://dx.doi.org/10.1016/j.isprsjprs.2015.04.013

**Table 8**
Optimized noise, multiple solutions and validation statistics (*RMSE* and $R^2$) and processing speed for each cost function. Results are ranked according to $R^2$.

| Cost function | % Noise | % Multiple solutions | *RMSE* | $R^2$ | Processing speed (s) |
|---|---|---|---|---|---|
| Pearson chi-square | 15 | 0.50 | 0.802 | 0.745 | 0.331 |
| Jeffreys–Kullback–Leibler | 18 | 0.50 | 0.799 | 0.734 | 0.473 |
| L-divergence lin | 16 | 0.25 | 0.794 | 0.734 | 0.757 |
| Shannon (1948) | 16 | 0.25 | 0.794 | 0.734 | 0.903 |
| Bhattacharyya divergence | 15 | 0.25 | 0.795 | 0.734 | 0.427 |
| Neyman chi-square | 18 | 0.25 | 0.806 | 0.717 | 0.334 |
| Least absolute error | 20 | 0.25 | 0.875 | 0.690 | 0.312 |
| Normal distrubution-LSE | 13 | 0.50 | 0.865 | 0.677 | 0.325 |
| Geman and McClure | 13 | 0.50 | 0.865 | 0.677 | 0.360 |
| Exponential | 13 | 0.50 | 0.868 | 0.674 | 0.445 |

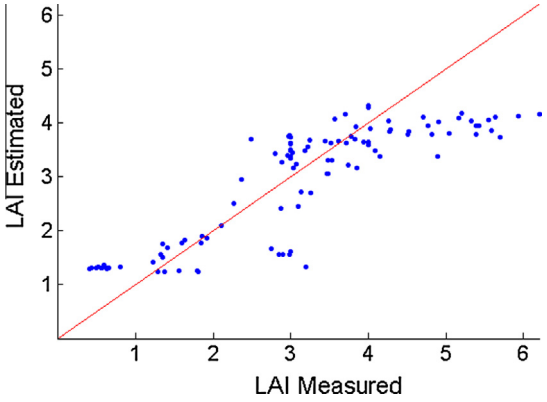


**Fig. 4.** Measured vs. estimated LAI values along the 1:1-line of the best LUT-based inversion scheme (see Table 8).

### 5.4. Final LAI maps

The best performing retrieval strategy for each retrieval category (parametric, non- parametric and physically-based) have been applied to map simulated Sentinel-2 imagery. Additionally, processing time to generate a map has been recorded. They are listed in Table 9. Large differences between the three methods were obtained. Due to its simplicity, retrievals based on vegetation indices are extremely fast. It takes less than 4 s to generate a map. The machine learning VH-GPR approach, led to the most accurate performance. Its sophisticated retrieval method, however, led to a slower mapping speed (1 min and 14 s), though 3 maps were generated in that time lapse (i.e. mean estimate, absolute uncertainty and relative uncertainty map). On the other hand, LUT-based inversions took considerably more time to generate the same map, i.e., 1 h, 1 min and 47 s. The slow mapping speed is due to the pixel-by-pixel evaluation with LUT entries. This low processing time is a significant drawback, e.g., in cases of operational applications or when maps are required in near real-time.

The LAI map as generated by the optimized 3BSI Tian index is shown in Fig. 5. In the obtained map the irrigated circular agricultural fields are clearly differentiated, including within-field variability. The non-vegetated areas are marked by LAI close to zero.

**Table 9**
Best performing parametric, non-parametric and LUT-based inversion method and associated mapping speed.

| Retrieval algorithm | *RMSE* | $R^2$ | Mapping speed (s) |
|---|---|---|---|
| Tian 3-band formulation | 0.615 | 0.823 | 3.847 |
| VH-GPR | 0.436 | 0.902 | 73.884 |
| Pearson chi-square inversion | 0.802 | 0.745 | 3706.965 |

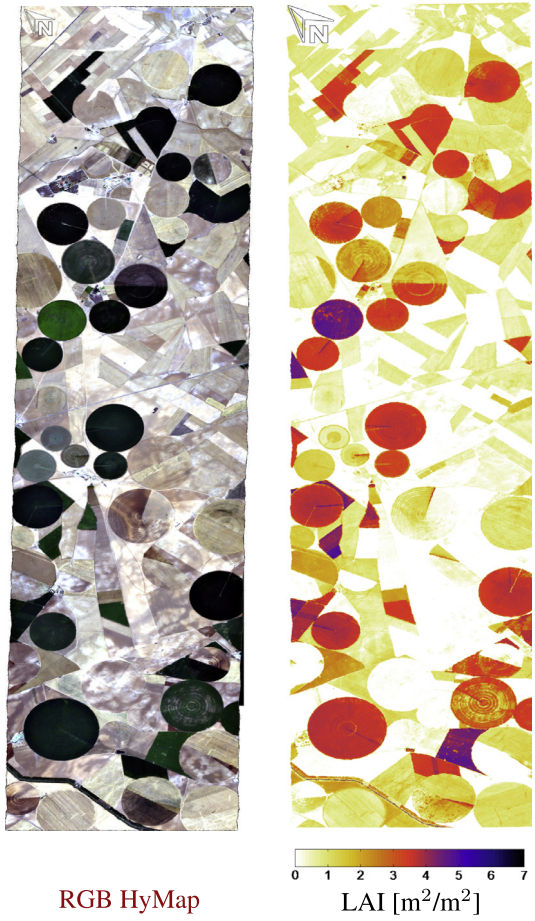


**Fig. 5.** S2 RGB map of the original HyMap flightline and LAI map as generated by the best performing vegetation index regression model (see Table 6). R: red (B4: 665 nm), G: green (B3: 560 nm), B: blue (B1: 443 nm). (For interpretation of the references to colour in this figure legend, the reader is referred to the web version of this article.)

While the obtained map seems to make physical sense, the problem inherent to vegetation indices is that no information about retrieval uncertainties is provided. Moreover, the validation dataset was taken only over vegetated areas. Hence, the validity of the map as a whole remains questionable. From all considered regression techniques, VH-GPR was evaluated to reach the highest accuracies. Moreover, thanks to its Bayesian backbone, the GPR family has unique additional features: (1) It reveals the most relevant bands for the development of the model (Fig. 3)). (2) It provides uncertainty intervals associated with the mean predictions ($\mu$) (Fig. 6).

Please cite this article in press as: Verrelst, J., et al. Experimental Sentinel-2 LAI estimation using parametric, non-parametric and physical retrieval methods – A comparison. ISPRS J. Photogram. Remote Sensing (2015), http://dx.doi.org/10.1016/j.isprsjprs.2015.04.013

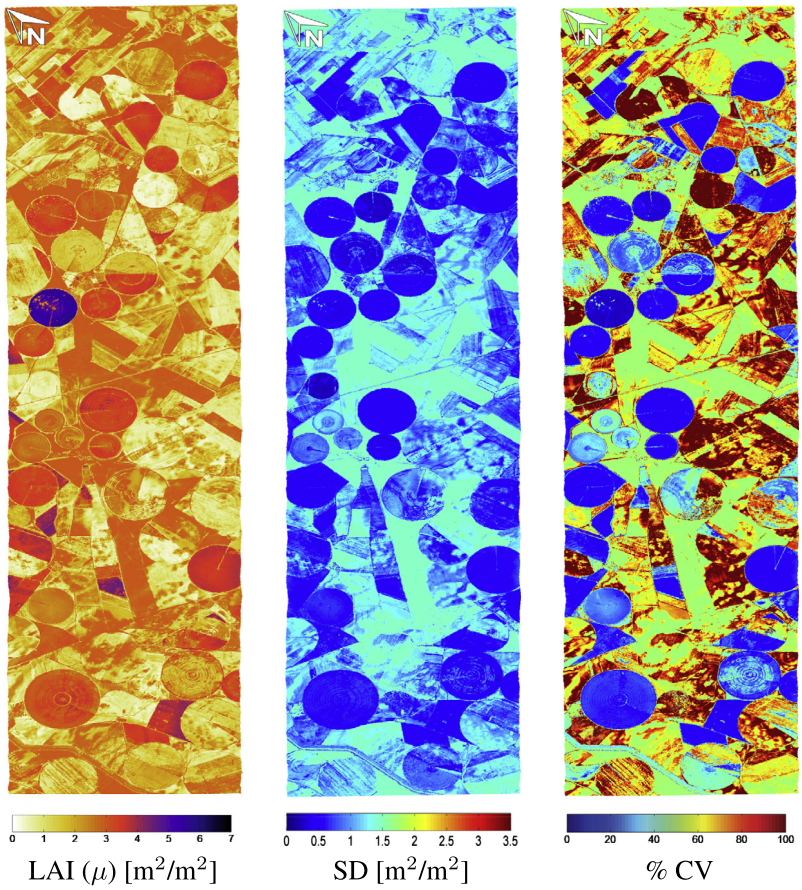


**Fig. 6.** LAI map (mean estimates; $\mu$) (left), associated uncertainties (expressed as standard deviation (SD) around the $\mu$) (centre), and relative uncertainties (expressed as coefficient of variation (CV $= \frac{SD}{\mu} * 100$) in %) (right) as generated by the best performing non-parametric regression model (see Table 9).

In the associated uncertainty map (Fig. 6, centre[1]), lower $\sigma$ (dark blue) indicates higher retrieval certainties from the trained model. The generation of uncertainty estimates allows insight into the pixel by pixel approach when applied to any imagery. It thus enables the interpretation for which land covers retrievals are associated with a large certainty and also those areas where land cover would benefit from additional sampling.

It should be kept in mind that $\sigma$ is also related to the magnitude of the mean estimates ($\mu$). For this reason relative uncertainties ($\sigma/\mu$) may provide a more meaningful interpretation. That map is also shown in Fig. 6 (right). It can be observed that LAI is retrieved with a high relative certainty over the circular areas. Typically, relative uncertainties below 20% are achieved for several of those areas, which falls within the accuracy threshold as proposed by Global Climate Observing System (GCOS) (GCOS, 2011). Note that on the fallow areas or bare soils, retrievals have a rather high relative uncertainty. By applying a threshold those more uncertain retrievals can be masked out. Hence, uncertainty maps can function as a spatial mask that enables displaying only pixels with a high certainty.

Finally, the LAI map as generated by LUT-based inversion is shown in Fig. 7. The same circular fields can be observed, though in general a much more homogeneous map is generated, particularly over the non-irrigated areas (cf. Fig. 7). It may however not be a surprise that the inversion approach faced difficulties over non-vegetated areas since the LUT was only prepared by the vegetation model PROSAIL. Uncertainty indicators were obtained through mapping of residues in the spectral space. The residues indicate the distance between the spectral observation and the best spectral simulation found in the LUT (here, mean of multiple solutions). The smaller the residue the better the achieved match, and thus confidence of the retrieval. Interestingly, this map shows much more spatial variation than the LAI retrievals, and resembles closely the VH-GPR uncertainty map. The irrigated, green areas were again retrieved with high confidence, while the bare soils and fallow lands were retrieved with a high uncertainty.

## 6. Discussion

The upcoming Sentinel-2 (S2) missions open opportunities to implement novel retrieval algorithms in operational processing chains. Of prime interest are accurate, fast, robust, and sufficiently flexible retrieval algorithms that make full use of the new S2 MSI bands. In Verrelst et al. (this issue) qualitative features of parametric, non-parametric, physical and hybrid methods have been evaluated. In this paper we employed a systematic and quantitative evaluation study of these methods with respect to retrieval accuracy and processing speed. This was enabled by using the same S2 band settings, retrievable variable (LAI) and a validation dataset that spans a diversity of crop types. In a related study (Verrelst et al., 2012b) the trade-off between gain in spectral information at the expense of spatial detail for the different S2 configurations (10, 20 and 60 m) has been investigated. Such varying spatial resolution was not considered in this study.

[1] For interpretation of color in Fig. 6, the reader is referred to the web version of this article.

Please cite this article in press as: Verrelst, J., et al. Experimental Sentinel-2 LAI estimation using parametric, non-parametric and physical retrieval methods – A comparison. ISPRS J. Photogram. Remote Sensing (2015), http://dx.doi.org/10.1016/j.isprsjprs.2015.04.013

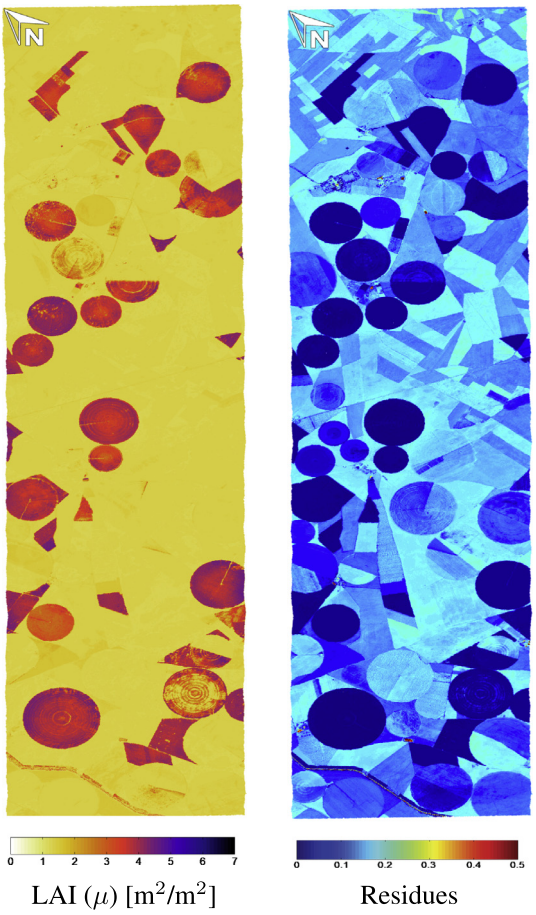


**Fig. 7.** LAI map (mean estimates; $\mu$) (left), associated residues (right) as generated by the best-performing LUT-based inversion scheme (see Table 7).

The greatest strength of parametric methods, such as vegetation indices, is their arithmetic simplicity, which leads to very fast processing and mapping speeds. Concomitantly, this simplicity has its limitations (see Verrelst et al. (this issue)). As demonstrated here, these boil down to a limited predictive performance. The best two-band index resulted into a $R^2_{CV}$ of 0.74. In fact, when multiple bands are available there is no reason to limit to two-band indices. For instance, it was demonstrated that three-band indices led to improved performance ($R^2_{CV}$ of up to 0.82). At the same time, although not examined here, it is to be expected that a systematic analysis of indices based on four or more bands will lead to further improvements. For instance, S2 enables 26,845 different four-band combinations.

To put the predictive power of vegetation indices in perspective with non-parametric methods, in an earlier study a multitude of published as well as generic indices were compared using Gaussian processes regression (GPR) (Verrelst et al., 2012a). It was concluded that there is no need to calculate a vegetation index prior to entering a GPR when the same bands can be directly entered into the GPR. The individual bands entered into GPR always led to superior results. Effectively, when moving away from parametric to non-parametric methods, a selection of bands, formulation or fitting function no longer has to be made. These algorithms have the capability to directly exploit the full spectrum. Particularly the nonlinear MLRAs proved to be very efficient. Prediction accuracies of $R^2_{CV}$ up to 0.90 were achieved at a relatively fast processing speed, i.e. in the order of seconds.

From the tested MLRAs feedforward neural networks (NNs) are probably the best-known and many space agencies and monitoring services already make use of NNs for operational products (Pozdnyakov et al., 2005; Schiller and Doerffer, 2005; Verger et al., 2008, 2011). It remains nevertheless to be questioned whether NNs are the most adequate algorithms to fulfill all these requirements. In this paper, various alternative MLRAs appeared to outperform NNs. Although more sophisticated types of NNs exist (e.g. recurrent artificial NN or radial basis function NNs), feedforward NNs face two known disadvantages:

1. They require a relatively long processing time to train a model;
2. They behave relatively unpredictable when used with input spectra deviating from those presented during the training stage (Kimes et al., 1998; Atzberger, 2004; Baret and Buis, 2008).

Beyond NNs, the family of GPR was evaluated as a promising regression algorithm in terms of processing speed and accuracy. Being based on a Bayesian framework, GPR provides insight in bands carrying relevant information and also in theoretical uncertainty estimates. As demonstrated earlier in Verrelst et al. (2013a) these uncertainties proved to be a useful tool for the assessment of upscaling capabilities of bio-geophysical variables from airborne or spaceborne platforms and their respective scales. Additionally, the associated uncertainty estimates also provide information on the success of transporting a locally trained model to other sites and/or observation conditions (Verrelst et al., 2013b). On the other hand, theoretical uncertainties are not intended to replace true accuracy estimates of the biophysical parameter products but instead provide complementary information. Physical accuracy estimates are mandatory and should be provided using comprehensive validation datasets collected on various sites, such as those coordinated by the Committee on Earth Observation Satellites (CEOS) Land Product Validation (LPV) community (Morisette et al., 2006).

When moving from statistical towards physical retrieval methods, the evaluation of various cost functions and regularization options lead to identified inversion strategies with best accuracies in terms of $R^2$ in the order of 0.74. These accuracies are below those of statistical methods.

It should be emphasized that inversion relies on simulated data with a turbid medium RTM as boundary condition (i.e. PROSAIL). Geometric RTMs have not been considered in this paper. The validation dataset included row crops such as maize, potatoes, onions and vineyards. In related works (Darvishzadeh et al., 2008; Richter et al., 2009) it was concluded that PROSAIL fails to invert for a multi-species canopy covering row crops. Moreover, various types of uncertainties have been identified leading to suboptimal retrievals with respect to model usage (e.g., 1 D vs. 3 D models), parametrization and validation data (Combal et al., 2003). Suggestions for improvements typically refer to the addition of prior information at the level of individual parcels (e.g. Atzberger, 2004; Combal et al., 2003; Knyazikhin et al., 1998; Meroni et al., 2004; Richter et al., 2009; Verrelst et al., 2012c). On the other hand, while such strategies could be beneficial for dedicated sites, site-specific information is usually unavailable for larger areas in an operational context. The applied regularization options yield inversion schemes easily applicable over full scenes that cover heterogeneous canopy surfaces. Performance gain is typically reached in combination with the application of a noise component and relying on the mean of multiple best solutions (Rivera et al., 2013; Verrelst et al., 2014). In a recent related study by Atzberger et al. (2015), however, a similar exercise was employed where LUT-based inversion was compared against vegetation indices and hybrid methods. There it was concluded that

Please cite this article in press as: Verrelst, J., et al. Experimental Sentinel-2 LAI estimation using parametric, non-parametric and physical retrieval methods – A comparison. ISPRS J. Photogram. Remote Sensing (2015), http://dx.doi.org/10.1016/j.isprsjprs.2015.04.013

inversion approaches possess several advantages such as good accuracy and being generic. Higher accuracies were obtained, probably because of spending more efforts on LUT configuration, using a larger LUT size (100,000 entries) and a band selection strategy. At the same time also the drawbacks were addressed, i.e. the need for an appropriate RTM, information for model parameterization, computing skills and computational resources.

As with GPR, an advantage of LUT-based inversion is the delivery of uncertainty estimates. Interestingly, while the LUT-based uncertainty estimates are obtained through different mechanisms, the inversion uncertainty indicators show a spatial trend consistent with that of GPR uncertainties. For the RTM inversion, pixels of vegetated surfaces match closely with the simulated reflectance database, while pixels of non-vegetated surfaces face more difficulties. Two reasons can be identified for this discrepancy: (1) The inversion scheme is optimized against validation data, exclusively collected for vegetated areas. (2) PROSAIL is a canopy reflectance model and thus only able to detect variations in vegetation properties. Consequently, a generated LUT and the final inversion scheme are not optimized to detect variations in fallow and bare soil lands. For retrievals on imagery with these types of land cover, there is a requirement to regulate the inversion procedure both for vegetated as well as non-vegetated targets. In practice, this requires extending the LUT with variables of soil profiles. This will, however, blow up the LUT size exponentially and hence significantly slow down processing speed. To overcome slow processing, alternative methods not requiring iteratively passing through a LUT, may be more successful, especially in an operational context. Such methodological approach can be found in the family of hybrid methods (Verrelst et al., this issue).

### 6.1. Towards a new generation of hybrid methods

Hybrid models exploit the generic properties of physically-based methods combined with the flexibility and computational efficiency of MLRA methods. The basic concept is to apply inverse mapping with a non-parametric model trained with simulated data generated with RTMs. Similarly as in LUT-based inversion, an RTM is used in direct mode to build the LUT representing a broad set of canopy realizations. Whereas a LUT approach seeks for a simulated spectrum as close as possible to the measured one, the hybrid approach uses all available data to train a MLRA. An important research question in this respect is how well the novel type of MLRAs performs, when fed with artificial spectra generated by an RT model.

Though hybrid strategies traditionally rely on the application of an NN, a few examples of more novel MLRAs are encountered in the scientific literature. Durbha et al. (2007) retrieved LAI from MISR data using a support vector regression (SVR) model trained with PROSAIL data. The same strategy was recently applied to estimate LAI from a HJ-CCD image (Pan et al., 2013). Doktor et al. (2014) used a PROSAIL dataset to train a random forest model to predict LAI and LCC. While some of the MLRA methods elicit advantages compared to NN structures (e.g. the models in a Bayesian framework), they are nonetheless still experimental and none of them have made it to operational applications yet.

Initial efforts in facilitating this approach have already been undertaken by implementing a MLRA module into the ARTMO toolbox, which consists of a suite (toolbox) of RTMs accessible by one GUI (Verrelst et al., 2012c). As such, MLRA models can be automatically developed with LUTs based on simulated spectra and their corresponding input parameters (e.g. LAI). Moreover, ARTMO allows to customize retrieval methods per land cover type. It is well understood that the models here optimized for croplands may not be the same ones as when optimizing retrieval algorithms for more heterogeneous land cover types such as natural vegetation or forest. Therefore, when having a land cover map available, ideally retrieval strategies should be customized per land cover type. At a global scale, LAI retrieval algorithms can be configured per biome or plant functional type, as is currently done for the MODIS LAI product (Myneni et al., 2002; Yang et al., 2006).

It should nonetheless be noted that, while novel types of MLRAs such as GPR are successful for small training datasets (e.g. <2000 samples), their computational load impedes the use of large datasets. This limitation has to be resolved when aiming at developing generic models for global applications. For instance, alternative (sparse) versions of GPR have been proposed that can cope with handling large scale datasets. Greedy algorithms in active learning settings can also be an alternative. For example, GPRs trained with different cross-validation sub-sampling provide a ranked list of the most informative spectra that can be used to generate a final model. Computationally lighter models such as KRR are able to cope better with large datasets. Forthcoming research will move in these directions and may ultimately reach a robust and generic retrieval scheme. A follow-up contribution will be dedicated to these novel hybrid schemes by evaluating MLRAs that are carefully trained (e.g. through active learning) with RTM data.

## 7. Conclusions

In preparation of the forthcoming availability of Sentinel-2 (S2) imagery, a systematic comparison of a multitude of parametric, non-parametric and physically-based retrieval methods using simulated S2 data has been performed. An experimental field dataset of biophysical data, collected at the agricultural site Barrax in Spain, was used to evaluate various retrieval methods on its ability to estimate leaf area index (LAI). This led to the following main findings:

Regarding parametric regression, there is no reason to believe that the widely used two-band indices are the optimal ones. The best performing index was a three-band index according to $(\rho_a - \rho_b - \rho_c)/(\rho_a + \rho_b + \rho_c)$ with its most sensitive bands in the green (560 nm) and the SWIR (1610, 2190 nm). Relatively accurate cross-validated performances for the validation points were reached ($R^2_{CV}$: 0.82; $RMSE_{CV}$: 0.62). However, saturation of LAI does still occur for LAI values above 5. The main strength of using spectral indices is that LAI mapping proceeded extremely fast. A limitation of parametric regression is that uncertainty estimates are not provided.

From the 11 tested non-parametric regression methods, the family of kernel machine learning regression algorithms performed optimally. The best performing algorithm belonged to the family of Gaussian processes regression (GPR) ($R^2_{CV}$: 0.90; $RMSE_{CV}$: 0.44). The algorithm functions within a Bayesian framework and provides probabilistic outputs, i.e. mean estimates and associated uncertainty intervals. Also kernel ridge regression (KRR) delivered excellent cross-validated accuracies ($R^2_{CV}$: 0.90; $RMSE_{CV}$: 0.45). Additionally, KRR was extremely fast in developing a model and processing an image. Conversely, the widely used partial least squares regression (PLSR) and neural networks (NN) were not performing optimally. Moreover, NN was rather slow when developing a model. Hence, it is recommended to replace these algorithms by more powerful ones.

LUT-based RTM inversion proved to be more challenging. First, an adequate RTM had to be chosen and a LUT created by parametrization of the input variables and boundary conditions. Each decision taken may impact the inversion performance. Various cost functions and regularization options were evaluated. Particularly the insertion of noise to account for uncertainties linked to measurements and models, improved the inversion process. Despite the optimization of the inversion process, the best performances were not better than an $R^2$ of 0.74 ($RMSE_{CV}$: 0.80).

Please cite this article in press as: Verrelst, J., et al. Experimental Sentinel-2 LAI estimation using parametric, non-parametric and physical retrieval methods – A comparison. ISPRS J. Photogram. Remote Sensing (2015), http://dx.doi.org/10.1016/j.isprsjprs.2015.04.013

The inversion procedure encountered difficulties with: (1) LAI overestimation for sparse vegetation and (2) LAI underestimation for dense vegetation. The first problem may be due to the lack of variability in used soil spectral profiles. The second problem is most probably due to saturation effects. The generation of LAI maps using LUT-based inversions was executed considerably slower than with the statistical algorithms (for example about 50 times slower than with GPR). This is due to the per-pixel iterative processing of the LUT for inversion purposes. An advantage is that retrieval uncertainty on estimates is provided through residues.

Comparing the three families of retrieval methods, it can be concluded that: (1) non-parametric methods, especially the kernel MLRAs, yielded the most accurate results and (2) parametric methods processed imagery the fastest for a vegetation bio-geophysical variable (LAI in this paper). Nevertheless, non-parametric methods processed imagery slower just in the order of seconds. Concomitantly, some MLRAs (family of GPR) provide uncertainty on the estimates. As a conclusion of this paper, given the availability of a (rich) field dataset, it is suggested that the family of kernel-based MLRAs (e.g. GPR) are the most promising algorithms when it comes to accurate and fast image processing for the mapping of vegetation bio-geophysical characteristics.

## Acknowledgments

This work was partially supported by the European Space Agency (ESA) Project 'FLEX/S3 Tandem Mission Performance Analysis and Requirements Consolidation Study (PARCS)', and by the Spanish Ministry of Economy and Competitiveness (MINECO) under Project LIFE-VISION TIN2012-38102-C03-01, and AYA2010-21432-C02-01. We thank the reviewers for their valuable suggestions.

## References

Alonso, L., Moreno, J., 2005. Advances and limitations in a parametric geometric correction of CHRIS/PROBA data. In: Proceedings of the 3rd CHRIS/Proba Workshop.

Atzberger, C., 2004. Object-based retrieval of biophysical canopy variables using artificial neural nets and radiative transfer models. Rem. Sens. Environ. 93 (1–2), 53–67.

Atzberger, C., Richter, K., 2012. Spatially constrained inversion of radiative transfer models for improved LAI mapping from future sentinel-2 imagery. Rem. Sens. Environ. 120, 208–218.

Atzberger, C., Darvishzadeh, R., Immitzer, M., Schlerf, M., Skidmore, A., le Maire, G., 2015. Comparative analysis of different retrieval methods for mapping grassland leaf area index using airborne imaging spectroscopy. Int. J. Appl. Earth Obs. Geoinf. (0)

Bacour, C., Baret, F., Béal, D., Weiss, M., Pavageau, K., 2006. Neural network estimation of LAI, fAPAR, fCover and LAI×Cab, from top of canopy MERIS reflectance data: principles and validation. Rem. Sens. Environ. 105 (4), 313–325.

Baret, F., Buis, S., 2008. Estimating canopy characteristics from remote sensing observations. Review of methods and associated problems. In: Liang, S. (Ed.), Advances in Land Remote Sensing: System, Modeling, Inversion and Application. Springer, pp. 171–200.

Berger, M., Moreno, J., Johannessen, J., Levelt, P., Hanssen, R., 2012. Esa's sentinel missions in support of earth system science. Rem. Sens. Environ. 120, 84–90.

Breiman, L., 1996. Bagging predictors. Mach. Learn. 24 (2), 123–140.

Breiman, L., Friedman, J., Stone, C., Olshen, R., 1984. Classification and Regression Trees. The Wadsworth and Brooks-Cole Statistics-probability Series. Taylor & Francis.

Camps-Valls, G., Gómez-Chova, L., Muñoz-Marí, J., Lázaro-Gredilla, M., Verrelst, J., 6 2013. simpleR: A Simple Educational Matlab Toolbox for Statistical Regression. V2.1. <http://www.uv.es/gcamps/code/simpleR.html>.

Clevers, J., Kooistra, L., 2012. Using hyperspectral remote sensing data for retrieving canopy chlorophyll and nitrogen content. IEEE J. Sel. Top. Appl. Earth Obs. Rem. Sens. 5 (2), 574–583.

Combal, B., Baret, F., Weiss, M., 2002. Improving canopy variables estimation from remote sensing data by exploiting ancillary information. Case study on sugar beet canopies. Agronomie 22 (2), 205–215.

Combal, B., Baret, F., Weiss, M., Trubuil, A., Macé, D., Pragnère, A., Myneni, R., Knyazikhin, Y., Wang, L., 2003. Retrieval of canopy biophysical variables from bidirectional reflectance using prior information to solve the ill-posed inverse problem. Rem. Sens. Environ. 84 (1), 1–15.

Darvishzadeh, R., Skidmore, A., Schlerf, M., Atzberger, C., 2008. Inversion of a radiative transfer model for estimating vegetation LAI and chlorophyll in a heterogeneous grassland. Rem. Sens. Environ. 112 (5), 2592–2604.

Darvishzadeh, R., Atzberger, C., Skidmore, A., Schlerf, M., 2011. Mapping grassland leaf area index with airborne hyperspectral imagery: a comparison study of statistical approaches and inversion of radiative transfer models. ISPRS J. Photogramm. Rem. Sens. 66 (6), 894–906.

Darvishzadeh, R., Matkan, A., Dashti Ahangar, A., 2012. Inversion of a radiative transfer model for estimation of rice canopy chlorophyll content using a lookup-table approach. IEEE J. Sel. Top. Appl. Earth Obs. Rem. Sens. 5 (4), 1222–1230.

Delegido, J., Verrelst, J., Alonso, L., Moreno, J., 2011. Evaluation of sentinel-2 red-edge bands for empirical estimation of green LAI and chlorophyll content. Sensors 11 (7), 7063–7081.

Delegido, J., Verrelst, J., Meza, C., Rivera, J., Alonso, L., Moreno, J., 2013. A red-edge spectral index for remote sensing estimation of green LAI over agroecosystems. Eur. J. Agron. 46, 42–52.

Doktor, D., Lausch, A., Spengler, D., Thurner, M., 2014. Extraction of plant physiological status from hyperspectral signatures using machine learning methods. Rem. Sens. 6 (12), 12247–12274.

Donlon, C., Berruti, B., Buongiorno, A., Ferreira, M.-H., Féménias, P., Frerick, J., Goryl, P., Klein, U., Laur, H., Mavrocordatos, C., Nieke, J., Rebhan, H., Seitz, B., Stroede, J., Sciarra, R., 2012. The global monitoring for environment and security (GMES) sentinel-3 mission. Rem. Sens. Environ. 120, 37–57.

Dorigo, W.A., Zurita-Milla, R., de Wit, A.J.W., Brazile, J., Singh, R., Schaepman, M.E., 2007. A review on reflective remote sensing and data assimilation techniques for enhanced agroecosystem modeling. Int. J. Appl. Earth Obs. Geoinf. 9 (2), 165–193.

Drusch, M., Del Bello, U., Carlier, S., Colin, O., Fernandez, V., Gascon, F., Hoersch, B., Isola, C., Laberinti, P., Martimort, P., Meygret, A., Spoto, F., Sy, O., Marchese, F., Bargellini, P., 2012. Sentinel-2: ESA's optical high-resolution mission for GMES operational services. Rem. Sens. Environ. 120, 25–36.

Durbha, S., King, R., Younan, N., 2007. Support vector machines regression for retrieval of leaf area index from multiangle imaging spectroradiometer. Rem. Sens. Environ. 107 (1–2), 348–361.

Feret, J.B., François, C., Asner, G.P., Gitelson, A.A., Martin, R.E., Bidel, L.P.R., Ustin, S.L., le Maire, G., Jacquemoud, S., 2008. PROSPECT-4 and 5: advances in the leaf optical properties model separating photosynthetic pigments. Rem. Sens. Environ. 112 (6), 3030–3043.

Fernández, G., Moreno, J., Gandía, S., Martínez, B., Vuolo, F., Morales, F., 2005. Statistical variability of field measurements of biophysical parameters in SPARC-2003 and SPARC-2004 campaigns. In: Proceedings of the SPARC Workshop.

Friedman, J., Hastie, T., Tibshirani, R., 2000. Additive logistic regression: a statistical view of boosting. Ann. Stat. 28 (2), 337–407.

Garrigues, S., Lacaze, R., Baret, F., Morisette, J., Weiss, M., Nickeson, J., Fernandes, R., Plummer, S., Shabanov, N., Myneni, R., Knyazikhin, Y., Yang, W., 2008. Validation and intercomparison of global leaf area index products derived from remote sensing data. J. Geophys. Res. G: Biogeosci. 113 (2).

GCOS, 2011. Systematic Observation Requirements for Satellite-Based Products for Climate, 2011 Update, Supplemental Details to the Satellite-Based Component of the Implementation Plan for the Global Observing System for Climate in Support of the UNFCCC (2010 update, GCOS-154), pp. 138.

Geladi, P., Kowalski, B., 1986. Partial least-squares regression: a tutorial. Anal. Chim. Acta 185 (C), 1–17.

Glenn, E., Huete, A., Nagler, P., Nelson, S., 2008. Relationship between remotely-sensed vegetation indices, canopy attributes and plant physiological processes: what vegetation indices can and cannot tell us about the landscape. Sensors 8 (4), 2136–2160.

Guanter, L., Alonso, L., Moreno, J., 2005. A method for the surface reflectance retrieval from PROBA/CHRIS data over land: application to ESA SPARC campaigns. IEEE Trans. Geosci. Rem. Sens. 43 (12), 2908–2917.

Hagan, M.T., Menhaj, M.B., 1994. Training feedforward networks with the Marquardt algorithm. IEEE Trans. Neural Netw. 5 (6), 989–993.

Hill, M., 2013. Vegetation index suites as indicators of vegetation state in grassland and savanna: an analysis with simulated sentinel-2 data for a North American transect. Rem. Sens. Environ. 137, 94–111.

Huang, G.-B., Zhu, Q.-Y., Siew, C.-K., 2006. Extreme learning machine: theory and applications. Neurocomputing 70 (1–3), 489–501.

Jacquemoud, S., Verhoef, W., Baret, F., Bacour, C., Zarco-Tejada, P., Asner, G., François, C., Ustin, S., 2009. PROSPECT + SAIL models: a review of use for vegetation characterization. Rem. Sens. Environ. 113 (SUPPL. 1), S56–S66.

Kimes, D.S., Nelson, R.F., Manry, M.T., Fung, A.K., 1998. Attributes of neural networks for extracting continuous vegetation variables from optical and radar measurements. Int. J. Rem. Sens. 19 (14), 2639–2662.

Knyazikhin, Y., Kranigk, J., Myneni, R., Panfyorov, O., Gravenhorst, G., 1998. Influence of small-scale structure on radiative transfer and photosynthesis in vegetation canopies. J. Geophys. Res. D: Atmos. 103 (D6), 6133–6144.

Laurent, V., Schaepman, M., Verhoef, W., Weyermann, J., Chavez, R., 2014. Bayesian object-based estimation of LAI and chlorophyll from a simulated sentinel-2 top-of-atmosphere radiance image. Rem. Sens. Environ. 140, 318–329.

Lazaro-Gredilla, M., Titsias, M., Verrelst, J., Camps-Valls, G., 2013. Retrieval of biophysical parameters with heteroscedastic gaussian processes. Geosci. Rem. Sens. Lett. IEEE PP (99), 1–5.

Please cite this article in press as: Verrelst, J., et al. Experimental Sentinel-2 LAI estimation using parametric, non-parametric and physical retrieval methods – A comparison. ISPRS J. Photogram. Remote Sensing (2015), http://dx.doi.org/10.1016/j.isprsjprs.2015.04.013

le Maire, G., François, C., Dufrene, E., 2004. Towards universal broad leaf chlorophyll indices using PROSPECT simulated database and hyperspectral reflectance measurements. Rem. Sens. Environ. 89 (1), 1–28.

Leonenko, G., North, P., Los, S., 2013. Statistical distances and their applications to biophysical parameter estimation: information measures, M-estimates, and minimum contrast methods. Rem. Sens. 5 (3), 1355–1388.

Liang, S., 2007. Recent developments in estimating land surface biogeophysical variables from optical remote sensing. Prog. Phys. Geogr. 31 (5), 501–516.

Malenovsky, Z., Rott, H., Cihlar, J., Schaepman, M., García-Santos, G., Fernandes, R., Berger, M., 2012. Sentinels for science: potential of sentinel-1, -2, and -3 missions for scientific observations of ocean, cryosphere, and land. Rem. Sens. Environ. 120, 91–101.

Meroni, M., Colombo, R., Panigada, C., 2004. Inversion of a radiative transfer model with hyperspectral observations for LAI mapping in poplar plantations. Rem. Sens. Environ. 92 (2), 195–206.

Morisette, J., Baret, F., Privette, J., Myneni, R., Nickeson, J., Garrigues, S., Shabanov, N., Weiss, M., Fernandes, R., Leblanc, S., Kalacska, M., Sánchez-Azofeifa, G., Chubey, M., Rivard, B., Stenberg, P., Rautiainen, M., Voipio, P., Manninen, T., Pilant, A., Lewis, T., Iiames, J., Colombo, R., Meroni, M., Busetto, L., Cohen, W., Turner, D., Warner, E., Petersen, G., Seufert, G., Cook, R., 2006. Validation of global moderate-resolution LAI products: a framework proposed within the CEOS land product validation subgroup. IEEE Trans. Geosci. Rem. Sens. 44 (7), 1804–1814.

Moulin, S., Bondeau, A., Delécolle, R., 1998. Combining agricultural crop models and satellite observations: from field to regional scales. Int. J. Rem. Sens. 19 (6), 1021–1036.

Myneni, R., Hoffman, S., Knyazikhin, Y., Privette, J., Glassy, J., Tian, Y., Wang, Y., Song, X., Zhang, Y., Smith, G., Lotsch, A., Friedl, M., Morisette, J., Votava, P., Nemani, R., Running, S., 2002. Global products of vegetation leaf area and fraction absorbed par from year one of modis data. Rem. Sens. Environ. 83 (1–2), 214–231.

Pan, J., Yang, H., He, W., Xu, P., 2013. Retrieve leaf area index from HJ-CCD image based on support vector regression and physical model. In: SPIE Proceedings, vol. 8887, p. 10.

Pozdnyakov, D., Shuchman, R., Korosov, A., Hatt, C., 2005. Operational algorithm for the retrieval of water quality in the Great Lakes. Rem. Sens. Environ. 97 (3), 352–370.

Rasmussen, C.E., Williams, C.K.I., 2006. Gaussian Processes for Machine Learning. The MIT Press, New York.

Richter, K., Atzberger, C., Vuolo, F., Weihs, P., D'Urso, G., 2009. Experimental assessment of the sentinel-2 band setting for RTM-based LAI retrieval of sugar beet and maize. Can. J. Rem. Sens. 35 (3), 230–247.

Richter, K., Atzberger, C., Vuolo, F., D'Urso, G., 2011. Evaluation of sentinel-2 spectral sampling for radiative transfer model based LAI estimation of wheat, sugar beet, and maize. IEEE J. Sel. Top. Appl. Earth Obs. Rem. Sens. 4 (2), 458–464.

Rivera Caicedo, J., Verrelst, J., Alonso, L., Moreno, J., Camps-Valls, G., 2014a. Toward a semiautomatic machine learning retrieval of biophysical parameters. IEEE J. Sel. Top. Appl. Earth Obs. Rem. Sens. 7 (4), 1249–1259.

Rivera Caicedo, J., Verrelst, J., Delegido, J., Veroustraete, F., Moreno, J., 2014b. On the semi-automatic retrieval of biophysical parameters based on spectral index optimization. Rem. Sens. 6 (6), 2866–2889.

Rivera, J., Verrelst, J., Leonenko, G., Moreno, J., 2013. Multiple cost functions and regularization options for improved retrieval of leaf chlorophyll content and LAI through inversion of the PROSAIL model. Rem. Sens. 5 (7), 3280–3304.

Schiller, H., Doerffer, R., 2005. Improved determination of coastal water constituent concentrations from MERIS data. IEEE Trans. Geosci. Rem. Sens. 43 (7), 1585–1591.

Schlemmera, M., Gitelson, A., Schepersa, J., Fergusona, R., Peng, Y., Shanahana, J., Rundquist, D., 2013. Remote estimation of nitrogen and chlorophyll contents in maize at leaf and canopy levels. Int. J. Appl. Earth Obs. Geoinf. 25 (1), 47–54.

Shannon, C.E., 1948. A mathematical theory of communication. Bell Syst. Tech. J. 27, 379–423.

Snee, R., 1977. Validation of regression models: Methods and examples. Technometrics 19 (4), 415–428.

Suykens, J., Vandewalle, J., 1999. Least squares support vector machine classifiers. Neural Process. Lett. 9 (3), 293–300.

Tian, Y.-C., Gu, K.-J., Chu, X., Yao, X., Cao, W.-X., Zhu, Y., 2013. Comparison of different hyperspectral vegetation indices for canopy leaf nitrogen concentration estimation in rice. Plant Soil, 1–17.

Tipping, M.E., 2001. The relevance vector machine. J. Mach. Learn. Res. 1, 211–244.

Verger, A., Baret, F., Weiss, M., 2008. Performances of neural networks for deriving LAI estimates from existing CYCLOPES and MODIS products. Rem. Sens. Environ. 112 (6), 2789–2803.

Verger, A.b., Baret, F., Camacho, F., 2011. Optimal modalities for radiative transfer-neural network estimation of canopy biophysical characteristics: evaluation over an agricultural area with CHRIS/PROBA observations. Rem. Sens. Environ. 115 (2), 415–426.

Verrelst, J., Alonso, L., Camps-Valls, G., Delegido, J., Moreno, J., 2012a. Retrieval of vegetation biophysical parameters using Gaussian process techniques. IEEE Trans. Geosci. Rem. Sens. 50 (5 PART 2), 1832–1843.

Verrelst, J., Muñoz, J., Alonso, L., Delegido, J., Rivera, J., Camps-Valls, G., Moreno, J., 2012b. Machine learning regression algorithms for biophysical parameter retrieval: opportunities for sentinel-2 and -3. Rem. Sens. Environ. 118, 127–139.

Verrelst, J., Romijn, E., Kooistra, L., 2012c. Mapping vegetation density in a heterogeneous river floodplain ecosystem using pointable CHRIS/PROBA data. Rem. Sens. 4 (9), 2866–2889.

Verrelst, J., Alonso, L., Rivera Caicedo, J., Moreno, J., Camps-Valls, G., 2013a. Gaussian process retrieval of chlorophyll content from imaging spectroscopy data. IEEE J. Sel. Top. Appl. Earth Obs. Rem. Sens. 6 (2), 867–874.

Verrelst, J., Rivera, J., Moreno, J., Camps-Valls, G., 2013b. Gaussian processes uncertainty estimates in experimental sentinel-2 LAI and leaf chlorophyll content retrieval. ISPRS J. Photogramm. Rem. Sens. 86, 157–167.

Verrelst, J., Rivera, J., Leonenko, G., Alonso, L., Moreno, J., 2014. Optimizing LUT-based RTM inversion for semiautomatic mapping of crop biophysical parameters from sentinel-2 and -3 data: role of cost functions. IEEE Trans. Geosci. Rem. Sens. 52, 257–269.

Verrelst, J., Camps Valls, G., Muñoz Marí, J., Rivera, J., Veroustraete, F., Clevers, J., Moreno, J., 2015. Optical remote sensing and the retrieval of terrestrial vegetation bio-geophysical attributes – a review. ISPRS J. Photogramm. Rem Sens. (this issue).

Vincini, M., Amaducci, S., Frazzi, E., 2014. Empirical estimation of leaf chlorophyll density in winter wheat canopies using sentinel-2 spectral resolution. IEEE Trans. Geosci. Rem. Sens. 52 (6), 3220–3235.

Wang, W., Yao, X., Yao, X., Tian, Y., Liu, X., Ni, J., Cao, W., Zhu, Y., 2012. Estimating leaf nitrogen concentration with three-band vegetation indices in rice and wheat. Field Crops Res. 129, 90–98.

Weiss, M., Baret, F., Myneni, R., Pragnère, A., Knyazikhin, Y., 2000. Investigation of a model inversion technique to estimate canopy biophysical variables from spectral and directional reflectance data. Agronomie 20 (1), 3–22.

Weiss, M., Baret, F., Garrigues, S., Lacaze, R., 2007. LAI and fAPAR CYCLOPES global products derived from VEGETATION. Part 2: Validation and comparison with MODIS collection 4 products. Rem. Sens. Environ. 110 (3), 317–331.

Wold, S., Esbensen, K., Geladi, P., 1987. Principal component analysis. Chemometr. Intell. Lab. Syst. 2 (1–3), 37–52.

Yang, W., Tan, B., Huang, D., Rautiainen, M., Shabanov, N., Wang, Y., Privette, J., Huemmrich, K., Fensholt, R., Sandholt, I., Weiss, M., Ahl, D., Gower, S., Nemani, R., Knyazikhin, Y., Myneni, R., 2006. MODIS leaf area index products: from validation to algorithm improvement. IEEE Trans. Geosci. Rem. Sens. 44 (7), 1885–1896.

Please cite this article in press as: Verrelst, J., et al. Experimental Sentinel-2 LAI estimation using parametric, non-parametric and physical retrieval methods – A comparison. ISPRS J. Photogram. Remote Sensing (2015), http://dx.doi.org/10.1016/j.isprsjprs.2015.04.013